MONITORING THE STATE OF THE COOLANT IN A BOILING WATER REACTOR

Graciela Roston, Robert Kozma, Masaharu Kitamura
Quantum Science and Energy Engineering Department
Tohoku University, Aramaki-Aza, Aoba, Sendai 980-77
JAPAN
Phone/Fax: +81-22-217-7907
E-mail: graciela@mine1.nucle.tohoku.ac.jp

Abstract

Transit time in a boiling water reactor is estimated using two methods: the displacement of the cross-correlation peak and the phase shift of the cross power spectral density. It has been observed that the transit time inferred from axially displaced neutron detectors does not satisfy a strict additive relationship. To see changes of the intensity of the void fraction fluctuations along the channel, we used a model based on the bimodal approximation in two-phase flows. A binormal fit of the probability density function (pdf) has also been performed.

Introduction

An important task of boiling water reactor (BWR) studies is a detailed description of the coolant flow condition in individual fuel bundles. When the coolant is a two-phase mixture of liquid and vapour, the coolant flow pattern can become quite complicated. In vertical two-phase flows, the following basic flow regimes can be defined: bubbly, slug, churn and annular.

A transit time can be associated with the axial propagation of the coolant density fluctuations. The measurement technique for transit time by means of cross-correlation of the signals (randomly time varying boiling noise pattern) of two axially displaced neutron detectors has been applied [1,2]. Both detectors are affected by the travelling disturbance, but the down stream signal is shifted with a time delay which is equal to the time for the disturbance to travel from the upstream detector to the down stream detector. A peak occurs in the cross-correlation function at the transit time *r* of the travelling disturbance. This is due to the definition:

$$Rxy = \frac{1}{T} \int_{-T2}^{T2} x(t) y(t+r) dt \tag{1}$$

The determination of the delay time between the two signals may also be performed in the frequency domain. The mathematically equivalent function is then the cross power spectral density (CPSD). The transit time in this case is given by the linear slope of the phase of this complex function:

$$CPSD(f) = [magnitude(f)] * exp) - i2\pi fr) \tag{2}$$

and

$$r = \frac{1}{2\pi} * \frac{d\theta}{dt} \tag{3}$$

where θ is the phase angle. The coherence function $\gamma^2(f)$ of two quantities $x(t)$ and $y(t)$ is defined as:

$$\gamma^2 = \frac{\left\| CPSD_{xy}(f) \right\|^2}{ASPD_x(f) * APSD_y(f)} \tag{4}$$

As this ordinary coherence function measures the extent to which $y(t)$ may be predicted from $x(t)$, in order to obtain an estimate of how the signal pattern changes between the two detectors, the coherence function was used.

The local power range monitors (LPRM) data have been represented by the corresponding probability density function (pdf). This function is the relative density with which the value *x* appears in the collection of data, and is an estimate of the rate of change of probability with magnitude [2].

The square of the root mean square RMS^2, which is the variance of the signal fluctuation, was calculated over an entire band between frequencies f_1 and f_2 as follows:

$$RMS_2 = \int_{f_1}^{f_2} APSD(f)df \tag{5}$$

It should be noted here that estimation of time delay by means of cross-correlation analysis is an established technique, if the quality of the observed signals is reasonably good. In our analysis with signals measured at a BWR, the measured variable is neutron fluctuation. Because of experimental limitations we can not install ordinary flow monitors (optical, impedance, etc.) inside the reactor. The neutronic signal can be disturbed not only by bubbles in the coolant flow but also by other quantities, e.g. temperature nonuniformity, flow regime, flow distribution within the coolant channel, etc. Detailed treatment of the fluctuations is needed in this regard.

Methodology

The data were taken from a 900MW BWR nuclear power plant at Forsmark I, Sweden. The measurement conditions were: reactor power: 64%, core flow: 4220 Kg/sec, Fs = 5 Hz. LPRM D, LPRM C, LPRM B and LPRM A are in the same string; LPRM D is in the top of the core, as is shown in Figure 1.

Figure 1. Reactor core and detector string

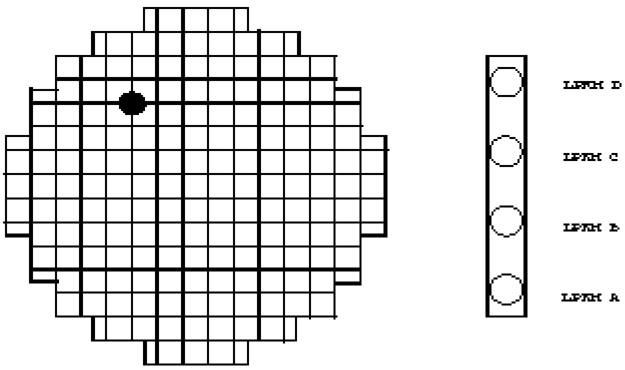

In general, an in-core detector will see the sum of local and global effects. With this in mind, we introduced a simple pre-processing of the signal. From each detector signal we subtracted the average of the four detectors in one string to remove global noise component. This analysis is denoted as ‘case (b)’, while the evaluations using the original time series are marked as ‘case (a)’.

For a given frequency range the coherence values were taken from:

$$\bar{\gamma}^2 = \frac{1}{f_1 - f_2} * \int_{f_2}^{f_1} \gamma^2 df \tag{6}$$

The phase angle was calculated in a frequency range corresponding to coherence values greater than 0.4.

For the calculation of the pdf of each signal, we took the half data points at the beginning and at the last, for a better comparison. Bubbly and annular flows have unimodal character, i.e. their pdf is single-peaked. Slug flows are classified as bimodal and they have pdf with two peaks. The modality of the flows is related to the moments of the pdf. This relation has been investigated [3] in order to develop an objective flow regime indicator. The assumption concerning spatial and temporal independence of bubbles is definitely not valid in slug flows, due to the presence of a well-defined spatial and temporal correlation in the void fraction fluctuation signal. Part of the difficulties can be solved by introducing a modified binomial model in which certain time-correlations are incorporated. The modified model is based on the bimodal approximation of void fraction fluctuations in two-phase flows [4]. We used this model in order to see changes of the intensity of the void fractions fluctuations along the channel. The bimodal two-phase flow model is determined by the following set of parameters: μ_1, μ_2, σ_1^2 and σ_2^2 which are the expected values and variance of the first and second mode respectively. The variance of the bimodal mixture is the sum of weighted variances of the separate modes and an additional term, which depends on the difference between the expected values of the two modes and on their relative frequency of occurrence. In order to develop an objective indicator, eliminating the characteristic constant and the background of each detector, we calculate:

$$z = \frac{(\mu_1 - \mu_2)^2}{\sigma_1^2 - \sigma_2^2} \qquad (7)$$

Based on this much-simplified model, in a meaningful range, *z* is a two-phase flow structure parameter. It contains information about the maximum possible number of bubbles in the sensitivity volume of the detector and it is a function of the void fraction of the two modes [4].

Observations

In Figure 2 and Figure 3 the coherence and phase between two LPRM are given for case (a) without subtraction, on the left side, and case (b) on the right side. When applying case (b) we get a better linearity in the phase, mainly at frequencies higher than 1 Hz. Also the frequency band of coherence values higher than 0.4 is larger. While approaching the bottom of the core, the phase is not linear (it has some peculiar fluctuations) and the coherence values are lower than 0.4 Hz. In Figure 3 the phase between LPRM B and LPRM D shows two different and well-defined slopes. For both cases, and between all the LPRM, the calculation and analysis clearly show that a core resonance phenomenon leads to oscillations at 0.5 Hz which are representative of the well-known BRW stability problem [5].

Figure 2. Coherence and phase for LPRM C and D

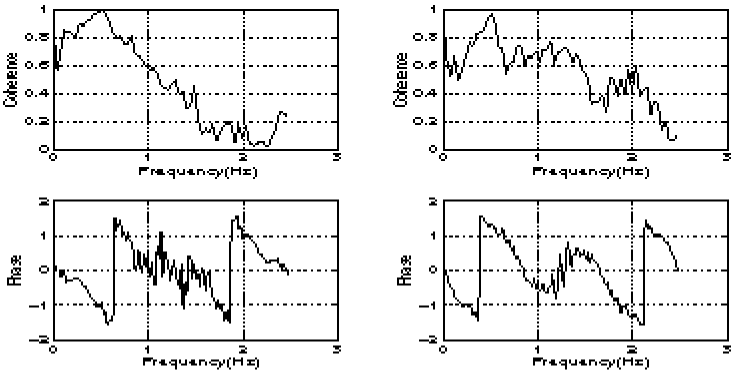

Figure 3. Coherence and phase for LPRM B and D

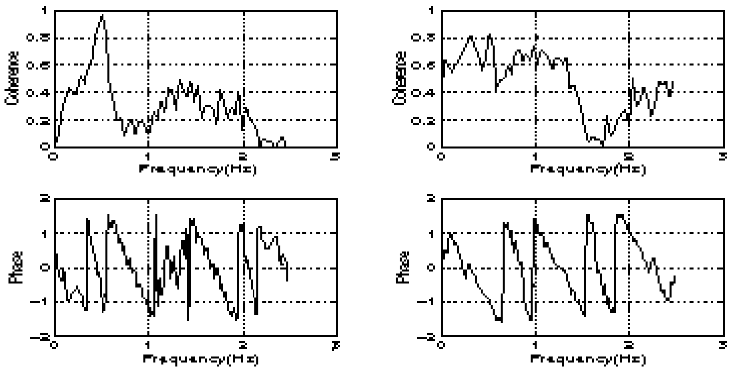

Table 1 shows the obtained time delay for different frequency bands, taking into account the coherence values. From this table, we can see that the correspondent results for both cases significantly differ for frequencies higher than 1 Hz.

Table 1. Time delay for LPRM D and LPRM C

Freq. Band (Hz)		Coherence		T (sec)	
Case (a)	Case (b)	Case (a)	Case (b)	Case (a)	Case (b)
0 : 0.63	0: 0.35	0.867	0.683	0.37	0.31
0.63 : 1.1	0.35 : 1.2	0.695	0.729	0.51	0.44
1.1 : 1.4	1.2 : 2.1	0.430	0.495	0.65	0.36

Table 2 summarises the calculation on the four detectors using the phase angle and the cross-correlation. In the first method, we took the mean weighted by both the frequency band and the coherence values along all the frequencies to compare these values with those obtained from the latter one. Only in case (b), we could calculate the time delay using the displacement of the cross-correlation peak.

Table 2. Time delay calculation on the 4 LPRM

Signal	Phase Case (a)	Phase Case (b)	Cross-Correlation
LPRM	Mean	Mean	Case (b)
C and D	0.48	0.376	0.2
B and C	0.411	0.417	0.4
B and D	–	0.900	0.8
A and B	0.740	0.345	0.4
A and C	–	0.75	1.0
A and D	–	0.610	1.4

The results obtained applying the displacement of the cross-correlation peak do not fulfil the additivity of the transit time. Additivity means:

$$T_{12} + T_{23} = T_{13}$$

where T_{12} is the transit time measured between detectors 1 and 2 in the same string. The best approximation for the additivity of the transit time is observed at frequencies higher than 1 Hz or below 0.4 Hz.

Table 3 shows the time delay along the channel using the phase shift of the CPSD for case (b).

Table 3. Time delay along the channel

Signal	Freq. 0.1 Hz : 0.4 Hz	Freq. 0.6 Hz : 1 Hz	Freq. 0 : 2 Hz
LPRM DC	0.314	0.435	0.376
LPRM CB	0.404	0.404	0.417
LPRM DB	0.759	1.410	0.900

The RMS^2 has been determined over various frequency regions according to [5]. The results, which are shown in Table 4, significantly vary for different frequency regions. At low frequencies there is an increase in the RMS^2 while at high frequency range a decrease is observed.

Table 4. RMS^2 over various frequency regions

F (Hz)	LPRM D	LPRM C	LPRM B	LPRM A
0 : 0.19	2.89	2.96	8.70	18.97
0.19 : 0.78	102.87	103.09	97.50	88.59
0.78 : 2.46	7.73	7.39	7.27	5.34
0 : 2.46	113.49	113.44	113.47	112.90

In Figure 4, the result of binormal fit of the pdf of LPRM D is shown. Crosses denote points of the calculated pdf having 50 channels; solid line shows the binormal fit and punctuated lines indicate the two Gaussian component of the fit.

Similar fit has been performed for the other three LPRM and the results are summarised in Table 5. Here, the expected values and the variances in each mode change for different signals, and also between the first and last data points. Also, the parameter *z* exhibits a systematic change as a function of LPRM position.

Figure 4. Results of the binormal fit of the pdf for LPRM D

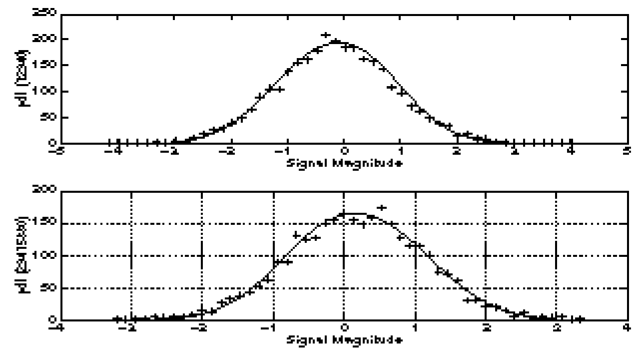

Table 5. Gaussian fitting of the four LPRM

	From pdf (1 : 2940)					From pdf (2941 : 5880)				
LPRM	μ_1	μ_2	σ_1	σ_2	z	μ_1	μ_2	σ_1	σ_2	z
D	0.4	-0.6	0.8	0.8	17	0.7	-0.3	0.8	0.8	16
C	0.3	-0.5	0.8	0.8	11	0.6	-0.4	0.8	0.8	12
B	0.6	-0.5	0.9	0.7	8	0.5	-0.4	0.9	0.7	7
A	0.6	-0.3	1	0.8	2	0.3	-0.5	0.9	0.7	3

Discussion

Due to the removal of the low frequency global noise, the frequency band of high coherence values greater than 0.4 increases. This effect also permits a better resolution in the linearity of the phase. Between LPRM D and LPRM A, due to the large spacing, the hydraulic turbulence and additional void generation practically wipe out bubble patterns over this distance. The mechanism responsible for the interesting fluctuations in the phase while approaching to the bottom of the core can not be explained at this point. Possibly due to the fact that LPRM signals oscillate in phase throughout the core and the strongest oscillation is found in the environment of 9x9 fuel (correspondent to the measured string) [5], the phase between LPRM D and LPRM B shows two different slopes. The decreasing of the RMS^2 at high frequencies (from the top to the bottom) can be understood on the basis of the bimodal two-phase flow model, where the RMS^2 at high frequencies is proportional to the void fraction [6]. In the framework of the study, at this point, it is difficult to find a reason to explain the changes of the expected values and the variances obtained from the bimodal fit for different signals and also between the first and last data point. Concerning the change of the parameter *z* along the channel, certainly, it depends on both the number of bubbles and the structure of the flow. For a better understanding of this parameter more study is needed.

Conclusions

The results obtained applying the displacement of the cross-correlation peak do not fulfil the additivity of the transit time. The best approximation for this additivity was obtained applying the coherence based frequency analysis of the phase shift of the CPSD. When the measured variable is neutron fluctuation, it is better to calculate the transit time for different frequencies, according to high coherence values, in order to get more reliable results. In our calculation, when the signal was pre-processed by removing the global noise component, the results were improved.

Acknowledgements

We are indebted to the Forsmark I Nuclear Power Plant, Sweden, for supplying us with measurement data and to Dr. Ritsuo Oguma from GSE Power Systems AB for useful discussions.

REFERENCES

[1] Thie J.: Power Reactor Noise, 159/163 American Nuclear Society (1981).

[2] Bendat J., Piersol A.: Random Data Analysis and Measurements Procedures, 48/50l, John Wiley and Sons (1986).

[3] Vince M. and Lahey R.: On the Development of an Objective Flow Regime Indicator. Int. J. Multiphase Flow, 8, 93/124 (1984).

[4] Kozma R.: Studies on the Relationship Between the Statistics of Void Fraction Fluctuations and the Parameters of Two-phase Flows. Int. J. Multiphase Flow, 21, 241/251 (1995).

[5] Bergdahl B., Reisch F., Oguma R.: BWR Stability Investigation at Forsmark I. Ann. Nucl. Energy. Vol. 16-10, 509/520 (1989).

[6] Kozma R., Kitamura M., Hoogenboom: Void Fraction Measurement in Nuclear Reactors Via Neutron Noise Methods. Paper submitted for publication (1995).